JOURNAL OF MATERIALS SCIENCE 29 (1994) 1239–1249

Sintering mechanisms and microstructural development of coprecipitated mullite

B. KANKA, H. SCHNEIDER
German Aerospace Establishment (DLR), Institute of Materials Research, 51140 Köln, Germany

Coprecipitated mullite precursor powders of the bulk compositions 78 wt % Al_2O_3 + 22 wt % SiO_2 (high-Al_2O_3 material) and 72 wt % Al_2O_3 + 28 wt % SiO_2 (low-Al_2O_3 material) have been used as starting materials. The precursor powders were calcined at 600, 950, 1000, 1250, and 1650° C, and test sintering runs were performed at 1550, 1600, 1650, 1700, and 1750° C. Homogeneous and dense ceramics were obtained from cold isostatically pressed (CIPed) powders sintered in air at 1700° C. Therefore, all further sintering experiments were carried out at 1700° C. After pressureless sintering, sample specimens were hot isostatically pressed (HIPed) at 1600° C and 200 bar argon gas pressure. Sintering densifications of low Al_2O_3 materials ranged between ≈94% and ≈95.5%. There was no clear dependency between densification and calcination temperature of the starting powders. High-Al_2O_3 compositions displayed sintering densities which increased from ≈97% at 600° C calcination temperature to ≈99% at 950° C calcination temperature. Higher calcination temperatures first caused slight lowering of the sintering density to ≈95.5% (calcination temperature 1250° C) but later the density strongly decreased to a value of 85% (calcination temperature 1650° C). HIPing of pressureless sintered specimens prepared from powders calcined between 600 and 1100° C yielded 100% density. At the given sintering temperature of 1700° C, the microstructure of sample specimens was influenced by Al_2O_3/SiO_2 ratios and by calcination temperatures of the starting powders. Homogeneous and dense microstructures consisting of equiaxed mullite plus some minor amount of α-Al_2O_3 were produced from high-Al_2O_3 powders calcined between 600 and 1100° C. Low-Al_2O_3 sample specimens sintered from precursor powders calcined between 600 and 1100° C were less dense than high-Al_2O_3 materials. Their microstructure consisted of relatively large and elongated mullite crystals which were embedded in a fine-grained matrix of mullite plus a coexisting glass phase. The different microstructural developments of high- and low-Al_2O_3 compositions may be explained by solid-state and liquid-phase sintering, respectively. The microstructure of HIPed samples was very similar to that of pressureless sintered materials, but without any pores occurring at grain boundaries.

1. Introduction

Mullite has become increasingly important as a high-temperature structural material in recent years, because it retains its room-temperature strength up to elevated temperature. Further favourable properties of mullite ceramics are the excellent creep resistance and a good thermal shock behaviour. The low thermal conductivity and expansion makes mullite suitable as a high-temperature insulating material. A new field of mullite application is its use as ceramic substrate. High-performance packaging for computer chips requires the development of ceramic materials with low dielectric constants, high wiring densities, and thermal expansion coefficients in the range of silicon. Furthermore, low sintering temperatures (≈ 1250 °C) for a possible cosintering with metals are necessary (for references, see [1]). Mullite ceramics are also preferred substrate materials in silicon solar cells for photovoltaic energy transformation (see, for example, [2,3]). Recent interest has been focused on the applicability of mullite ceramics as an infrared window material in the 3–5 μm wavelength region: Prochazka and Klug [4] were the first to describe infrared transparent mullite windows. It has been shown that the optical properties compare favourably with other ceramic materials (for further references, see [1]).

The immense importance of mullite in the field of traditional and advanced ceramics is documented in the enormous number of scientific and technical investigations which have been carried out in recent years. Of particular value for the understanding of the formation and properties of mullite materials are the basic publications of Pask and co-workers (e.g. [5, 6]). Other review papers on mullite ceramics were published by Somiya and Hirate [7] and by Aksay *et al.* [1], while Schneider [8] published a mineralogical

0022-2461

overview on mullite. Much of the recent progress in the improvement of mullite ceramics was the result of two special mullite conferences, one taking place in Tokyo (Japan) in November 1987, and the other one in Seattle (USA) in October 1990.

2. Material characterization

2.1. Dilatometer measurements

Dilatometer measurements were carried out with a conventional dilatometer in air, and with a dilatometer integrated in the hot isostatic press (HIP).

Conventional dilatometer runs in an air atmosphere were carried out in a difference dilatometer (Bähr, Thermo Analyser 802 SI), with an Al_2O_3 measuring system. Sample specimens were 3 mm × 3 mm × 6 mm in size. Length changes were measured in comparison to a dense α-Al_2O_3 sample specimen. A constant heating rate of 20 °C min^{-1} was used for the experiments with a Pt–PtRh(10%) thermocouple controlling the temperature to an accuracy of ± 5 °C.

The HIP integrated dilatometer runs were carried out in an argon atmosphere with a dilatometer adapted to the Asea Brown Bovery Q149 hot isostatic press. For the measurements, sample specimens of ≈ 10 mm × ≈ 10 mm × > 10 mm were used. Length changes were measured in comparison to those of runs without sample specimens. A constant heating rate of 20 °C min^{-1} was used with a WRe (5)–WRe (26) thermocouple measuring the temperature to an accuracy of ± 10 °C.

2.2 Density and powder surface measurements

Green densities were determined by measuring exactly the dimensions of the specimens, while bulk density measurements were carried out according to the Archimedes method using distilled water. Test bar sizes were typically ≈ 3.5 mm × ≈ 4.5 mm × > 40 mm. The relative densities were calculated using 3.15 g cm^{-3} as 100% in the case of low-Al_2O_3 compositions and 3.19 g cm^{-3} for high-Al_2O_3 materials.

Powder surface values were calculated using the Brunauer–Emmett–Teller (BET) technique with high-purity nitrogen after drying the powders at 250 °C in a nitrogen atmosphere for 2 h.

2.3. Microstructural observation and phase content

The microstructures of samples were examined with a scanning electron microscope (Philips SEM 525 M). Fracture surfaces and polished sections of chemically etched and unetched specimens have been investigated. Phase analyses were carried out with a computer-controlled powder diffractometer (Siemens D 5000) using nickel-filtered copper radiation. Diffractograms were recorded in the 10°–80° 2θ range in a step-scan mode (5 s/0.01°, 2θ).

3. Sample materials

The starting materials for the present study were provided by Hüls Company (Marl, Germany) in the

TABLE I Description of starting powders and of sintering properties

Al_2O_3 Composition		Calcination temperature [° C]				
		600 (15 h)	950 (5 h)	1100 (5 h)	1250 (15 h)	1650 (2 h)
High (78 wt%)	Weight loss during calcination (%)	21	30.5	31.4	31	32
	Phase content	Non-crystalline	Mullite	Mullite	Mullite + α-Al_2O_3	Mullite + α-Al_2O_3
	Surface area after calcination (g m^{-2})	72	70	55.6	23.6	3.1
	Green density of sample specimens (% theoretical density)	40.7	43.5	48	50	62
	Density after sintering (1700 °C, 4 h) (% theoretical density)	97.1	99	98.2	95.4	85
	Density after HIPing	≈ 100	≈ 100	≈ 100	98.8	[a]
Low (72 wt %)	Weight loss during calcination (%)	21.5	31	30.8	31.5	32.3
	Phase content	Non-crystalline	Mullite	Mullite	Mullite	Mullite
	Surface area after calcination (g m^{-2})	84	73	28.5	24.2	5.3
	Green density of sample specimens (% theoretical density)	41.5	44.6	48.2	51.7	62.0
	Density after sintering (1700 °C, 4 h) (% theoretical density)	94.5	95.5	93.8	94.4	95.3
	Density after HIPing	≈ 100	100	100	97.6	≈ 100

[a] insufficient pre-HIP density available

form of non-crystalline mullite precursor powders. The precursors were synthesized by coprecipitation of sodium aluminate and SiO_2 sol at pH = 7, with H_2SO_4 at about 50 °C. The starting materials were admixed in proportions corresponding to 78 wt % Al_2O_3 + 22 wt % SiO_2 (designated high-Al_2O_3 material) and 72 wt % Al_2O_3 + 28 wt % SiO_2) (designated low-Al_2O_3 material). The as-received coprecipitated materials were dried at 150 °C.

4. Powder processing and sintering

4.1. Powder processing

The as-received mullite precursor powders were calcined at 600, 950, 1100, 1250 and 1650 °C. Calcination produced weight losses up to 21.5 wt % at 600 °C, and up to 32.5 wt % at higher calcination temperatures (Table I). The strong weight losses are attributed essentially to the evaporation of water and to decomposition of sulphuric acid occurring in the precursors.

According to X-ray diffraction patterns, 600 °C samples are non-crystalline. Above about 950 °C mullitization is observed in high- and low-Al_2O_3 compositions. However, while mullite is the only crystalline phase in low-Al_2O_3 materials calcined between 950 and 1650 °C, some additional α-Al_2O_3 can be detected in high Al_2O_3 compositions calcined at 1250 and 1650 °C (Table I).

Surface-area measurements with BET showed that mullite precursor powders, calcined at relatively low temperature ($\leqslant$ 1100 °C) contained relatively large agglomerates up to 15 μm in size. Higher calcination temperatures ($\geqslant$ 1100 °C) produced very fine crystalline powders, however, with much lower surface areas (Table I). The calcined powders were milled at least 15 h, in order to crack agglomerates. Milling runs were performed in a polymer vessel, filled with 33 wt % mullite powder, 33 wt % Si_3N_4 milling balls (ball diameter 5 mm), and 33 wt % isopropanol.

To minimize internal stresses during pressing, and in order to increase green densities of sample specimens, 6 wt % of an oil–acid ($C_{16}H_{34}O_3$), or of a wax combination were admixed to the mullite powders. The powder oil–acid or wax admixtures were homogenized and later dried in a rotor vapour.

In a further step of processing, powders were sieved through a 100 mesh screen, and then compacted at 15 MPa into bars with the following dimensions: 63 mm × 5 mm × h mm (h = variable dimension). The shaping pressure was minimized in order to avoid pressing cone cracks. The die-pressed bars were vacuum sealed in thin-walled latex tubings, and then were isostatically cold-pressed (CIPed) at 250 MPa. After CIPing the organic binder was burned out carefully at temperatures up to 600 °C (heating rate 40 °C h^{-1}). Green densities of sample specimens dependent on changing calcination temperatures are given in Table I. There exists a strong correlation between green densities and calcination temperatures for both high- and low-Al_2O_3 compositions.

Figure 1 provides a flow sheet showing the different steps necessary for sample specimen preparation.

4.2. Sintering experiments

4.2.1. Pressureless sintering

Pressureless sintering runs were performed in an $MoSi_2$-heated computer-controlled chamber furnace (Ceram-Aix) in air. In order to find the best sintering temperatures, test sintering runs of differently pre-

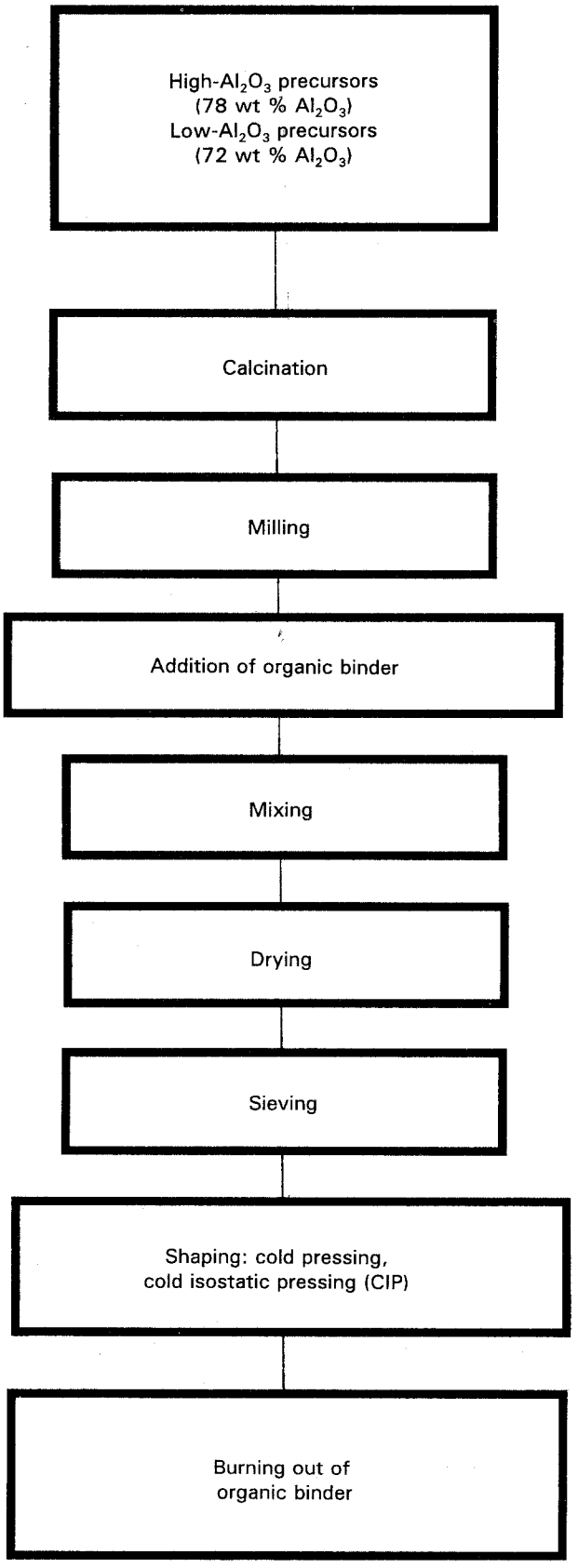

Figure 1 Powder processing routes for high-Al_2O_3 (78 wt % Al_2O_3) and low-Al_2O_3 (72 wt % Al_2O_3) precursor powders.

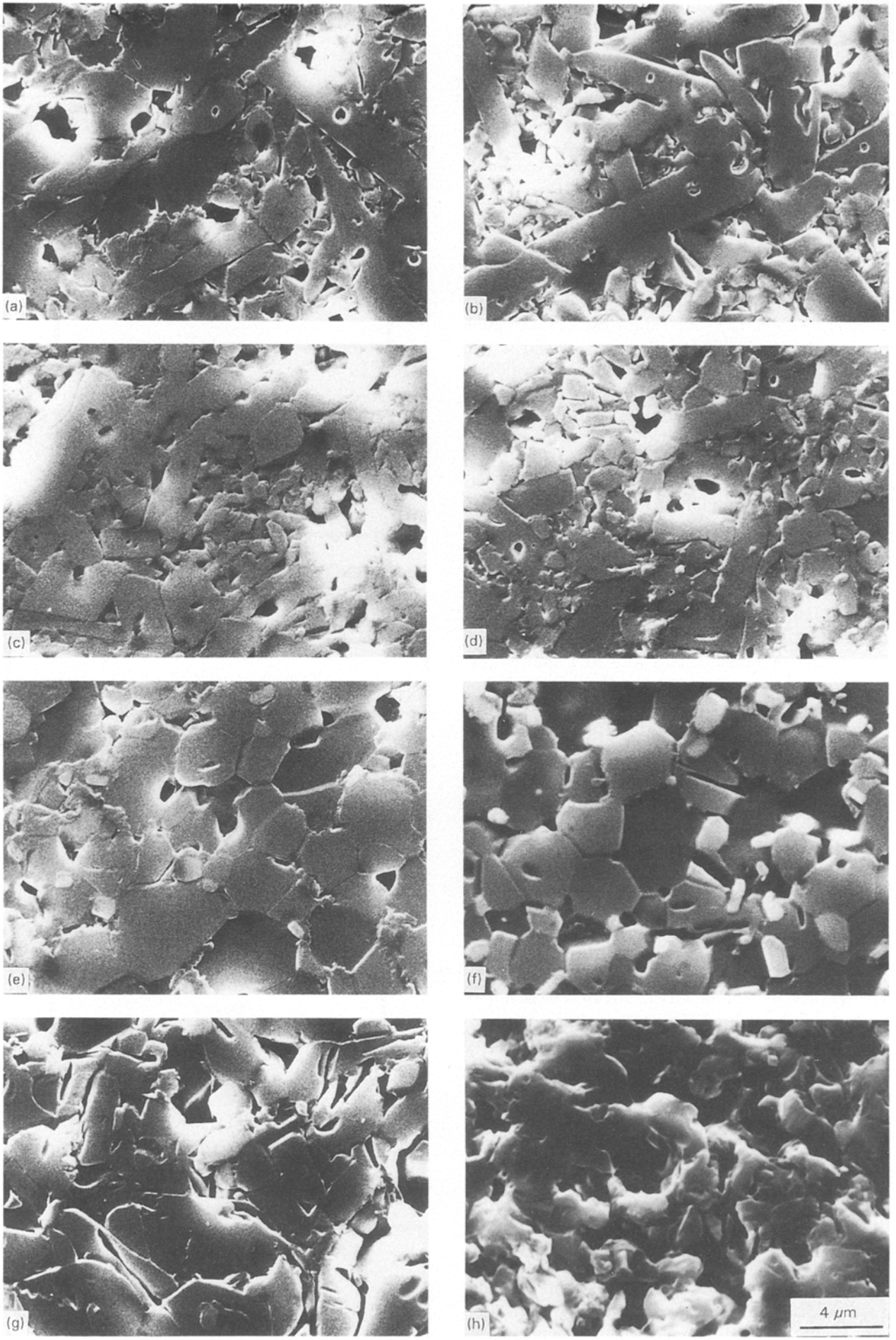

Figure 2 Scanning electron micrographs of (a–d) low-Al_2O_3 (72 wt % Al_2O_3) and (e–h) high-Al_2O_3 (78 wt % Al_2O_3) materials. Specimens are prepared from precursor powders calcined at (a, e) 600, (b, f) 950, (c, g) 1250, and (d, h) 1650 ° C, and are sintered at 1700 ° C in air. Chemically etched polished sections.

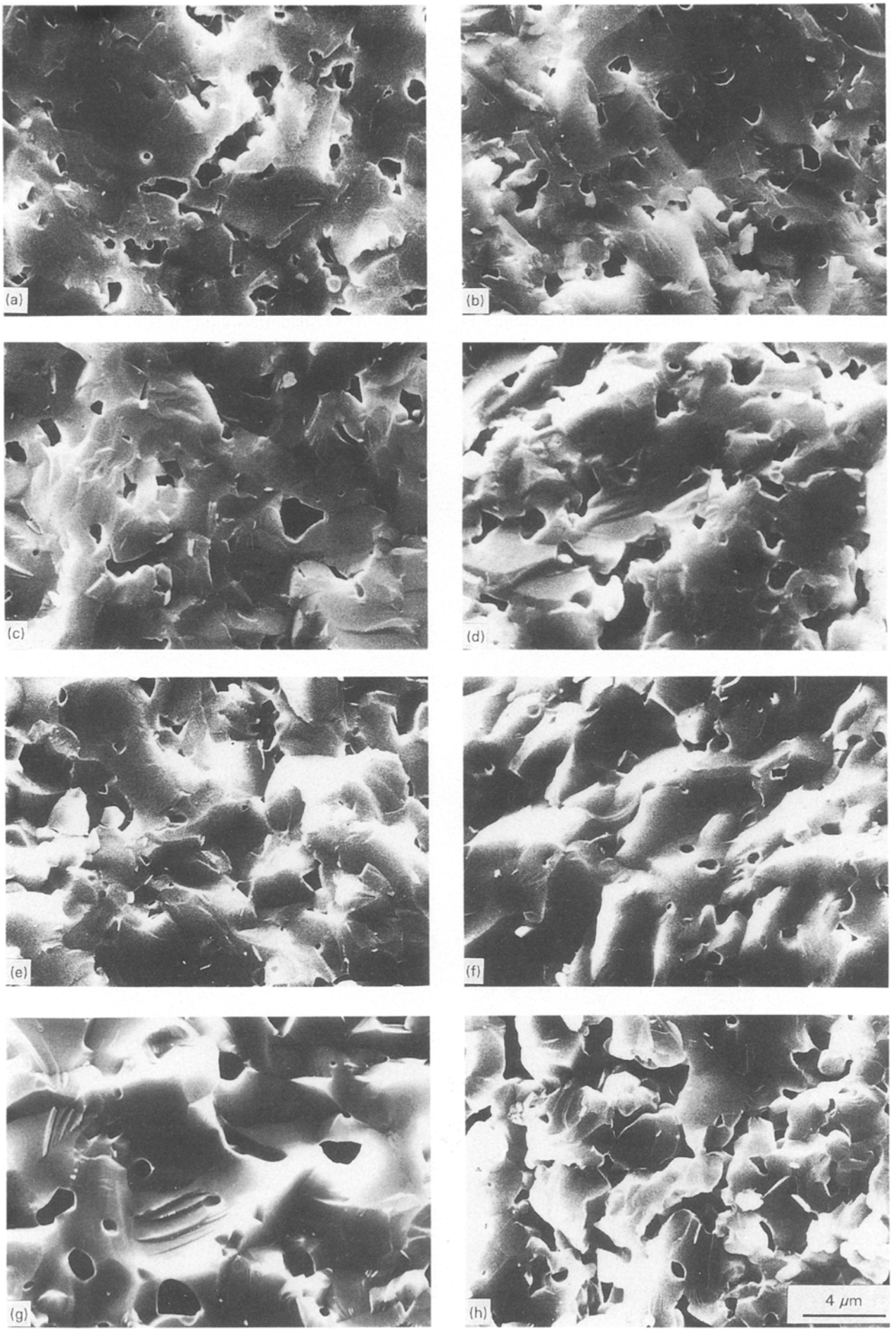

Figure 3 Scanning electron micrographs of (a–d) low-Al_2O_3 (78 wt % Al_2O_3) (e–h) high-Al_2O_3 (78 wt % Al_2O_3) materials. Specimens are prepared from precursor powders calcined at (a, e) 600, (b, f) 950, (c, g) 1250, and (d, h) 1650 ° C, and are sintered at 1700 ° C in air. Fracture surfaces.

calcined mullite powders were performed at 1550, 1600, 1650, 1700 and 1750 °C (heating rate 300 °C h^{-1}, holding time 4 h).

4.2.2. Hot isostatic pressing (HIPing)

HIP experiments were performed in an Asea Brown Bovery QJH9 hot isostatic press (HIP) with c/c heating elements. Presintered mullite samples were placed in an Al_2O_3 die. Sample specimens were embedded in a mullite–BN powder mixture, in order to prevent decomposition of mullite due to the reducing atmosphere in the HIP graphite furnace running in an argon atmosphere. Systematic variation of HIP pressures and temperatures yielded best HIP parameters at 1600 °C and 200 bar (argon gas pressure).

5. Microstructural development

5.1. Pressureless sintering

All microstructural studies were carried out on specimens sintered at 1700 °C for 4 h. High-Al_2O_3 materials calcined at 600, 950, and 1100 °C prior to sintering were rather homogeneous. Microstructures were characterized by equiaxed mullite crystals up to about 5 μm in size, and a low amount of small equiaxed α-Al_2O_3 grains, occurring at mullite–mullite grain boundaries (Fig. 2). Specimens made from precursor powders, calcined at 1250 °C, display more heterogeneous microstructures with elongated, rounded-up and frequently bended crystals. Mullite ceramics produced from precursors calcined at 1650 °C consist of relatively small mullite crystals. High Al_2O_3 materials first show a slight decrease of the porosity with a calcination temperature going from 600–950 °C. At higher calcination temperatures the porosity again increases. The porosity is especially high for sintering specimens produced from precursor powders calcined at 1650 °C (Fig. 3, see also Table I).

Low-Al_2O_3 materials contain relatively large and elongated mullite crystals, which are embedded in a finer-grained mullite matrix (Fig. 2). Grain sizes and aspect ratios of the elongated crystals have maxima in sample specimens produced from precursor powders calcined between 600 and 1100 °C (maximum size of elongated mullite crystals is about 5–15 μm). Size and aspect ratio of the elongated mullite crystals rapidly redecrease for higher calcination temperatures. The sizes of the smaller more equiaxed "matrix" mullite crystals were more or less constant (average size

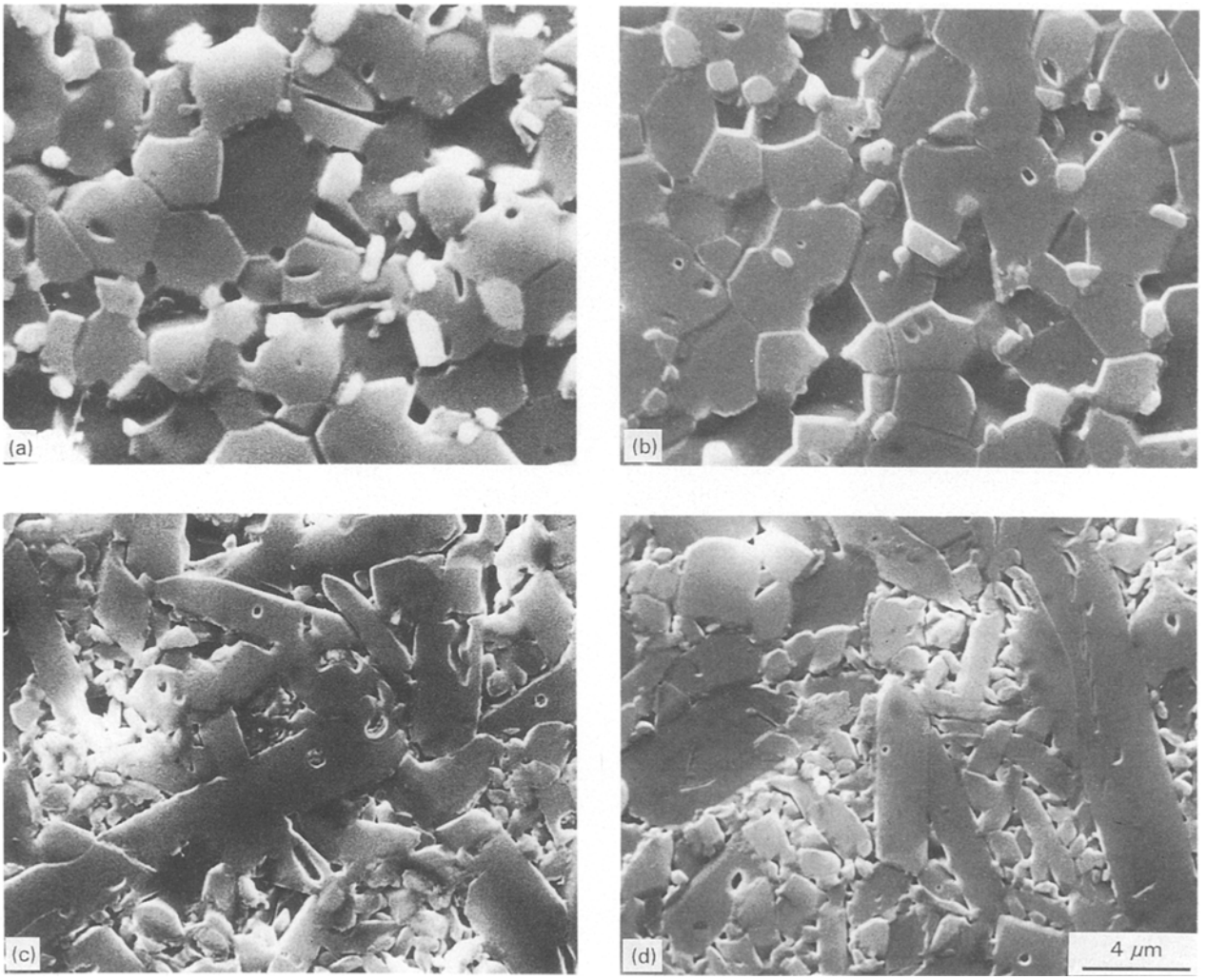

Figure 4 Scanning electron micrographs of (a, b) high-Al_2O_3 (78 wt % Al_2O_3) and (c, d) low-Al_2O_3 (72 wt % Al_2O_3) materials. Specimens are prepared from precursor powders calcined between 950 and 1100 ° C, and are (a, c) sintered at 1700 ° C in air, and (b, d) sintered + HIPed at 1600 ° C at 1200 bar argon pressure. Chemically etched polished sections.

0.5–3 μm) for all calcination temperatures. The large elongated mullite crystals often contained rounded-up pores. Pores also occurred between individual mullite grains. Microscopical observation and density measurements (Fig. 3 and Table I) indicate that bulk porosities of low-Al_2O_3 sample specimens do not change significantly with the calcination temperature.

5.2. Hot isostatic pressing (HIPing)

Fig. 4 shows scanning electron micrographs of HIPed high- and low-Al_2O_3 compositions in comparison to sintered but non-HIPed specimens. The microstructures of HIPed samples are very similar to those of the pressureless sintered mullite materials. The difference between both types of material is the content of pores occurring in both materials: the pore frequency at mullite–mullite grain boundaries in HIPed samples is drastically reduced with respect to that in non-HIPed samples, though some residual pores occur within individual mullite crystals also in the HIPed material.

6. Sintering behaviour

6.1. Pressureless sintering

The aim of pressureless sintering was to obtain dense ceramics with homogeneous microstructures. Sample specimens should be suitable for HIPing, i.e. they must have closed porosity only (i.e. $\geqslant 93\%$ theoretical density).

Preliminary sintering experiments were carried out between 1550 and 1750 °C on the differently calcined precursor powders, in order to determine the optimum sintering temperature. At 1550 °C, sample specimens produced from precalcined powders yielded low sintering densities, though there exists a reciprocal dependency between calcination temperature and sintering densification. With increase of the sintering temperature the degree of densification increases, but reaches a saturation value at 1700 °C. Powders precalcined at 1650 °C are an exception, in having low sintering densities up to 1750 °C (Fig. 5). It turns out that best densification conditions were achieved at a sintering temperature of 1700 °C. Therefore, all further sintering experiments were carried out at 1700 °C (see Section 4.2).

The calcination procedure of the as-received precursor powders has a controlling influence on the sintering behaviour of sample specimens (Table I). While low-Al_2O_3 compositions do not show any significant change of sintering densities, with a mean value near 94%, high-Al_2O_3 compositions first increase in density from $\approx 97\%$ at a calcination temperature of 600 °C to a value of $\approx 99\%$ at a calcination temperature of 950 °C. Above this temperature limit, densities first slightly, but later considerably decrease to reach a value of 85% at a calcination temperature of 1650 °C.

Dilatometer curves of high- and low-Al_2O_3 compositions (calcination temperature 1100 °C) measured under an oxidizing (air) atmosphere are given in Fig. 6. Sintering is initiated above about 1100 °C. Initially the

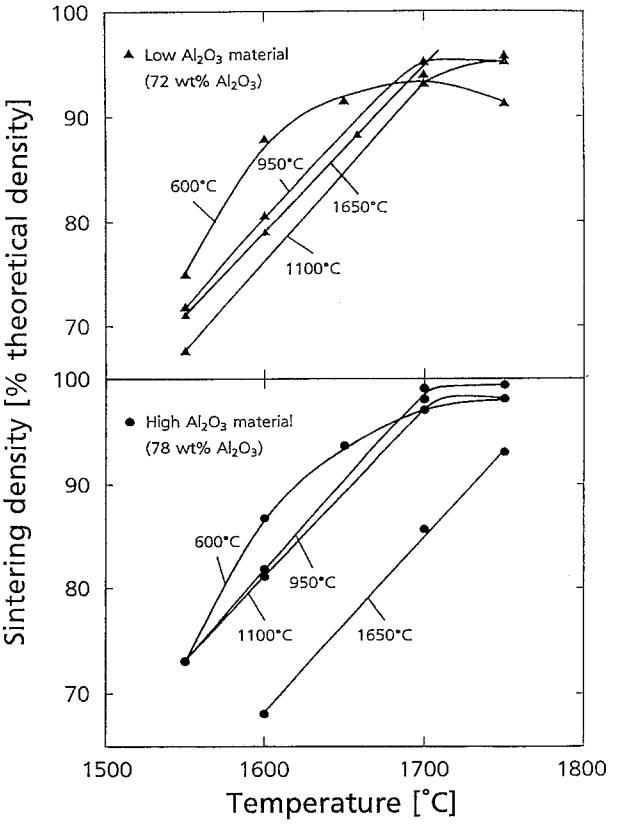

Figure 5 Sintering density of (●) high-Al_2O_3 (78 wt % Al_2O_3) and (▲) low-Al_2O_3 (72 wt % Al_2O_3) materials plotted versus increasing sintering temperature. Specimens are prepared from precursor powders calcined at 600, 950, 1100, and 1650 ° C.

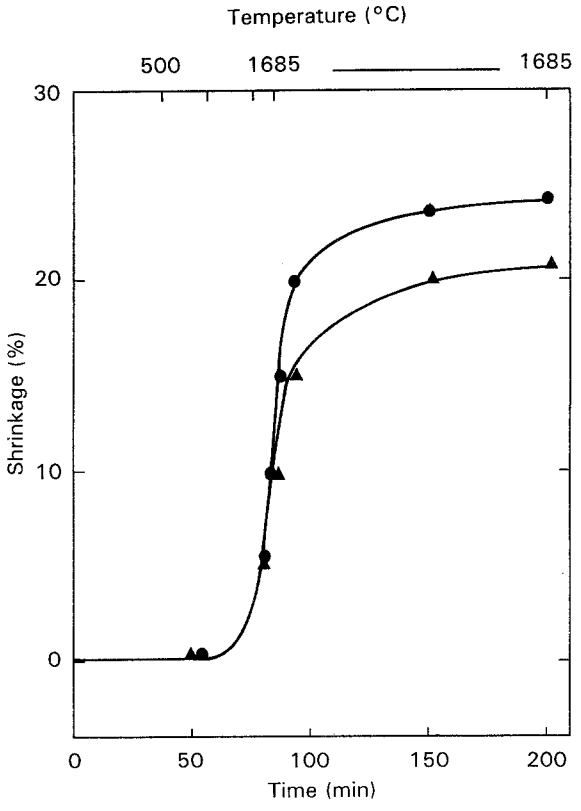

Figure 6 Densification curves of (●) high-Al_2O_3 (78 wt % Al_2O_3) and (▲) low-Al_2O_3 (72 wt % Al_2O_3) materials dependent on temperature and time. Specimens are prepared from precursor powders calcined at 1100 ° C. The curves were recorded in a dilatometer in air.

sintering rate of the low-Al_2O_3 materials is slightly higher than that of the high-Al_2O_3 composition. However, at higher temperatures above about 1400 °C, sintering rates are larger for high-Al_2O_3 compositions than for low-Al_2O_3 materials. High-Al_2O_3 compositions display higher final densities than low-Al_2O_3 materials.

6.2. Hot isostatic pressing (HIPing)

HIP experiments were performed in order to achieve 100% dense specimens. HIP-densification curves of high- and low-Al_2O_3 compositions (calcination temperature 1100 °C, sintering conditions 1700 °C, 4 h) are shown in Fig. 7. Low-Al_2O_3 materials, with pre-HIP densities of 93.8% exhibit low densification rates above about 1350 °C and up to about 1450 °C. Above this temperature limit and with longer HIPing runs, a considerable increase of densification up to theoretical density (100%) is observed.

High-Al_2O_3 materials with pre-HIP densities of 98.2% display no noticeable HIP densification up to about 1500 °C. Between 1500 and about 1600 °C weak HIP-induced sintering occurs. Beyond this point the sintering velocity increases, shrinking curves having similar slopes as for low-Al_2O_3 compositions. In spite of these similarities, high Al_2O_3 materials require longer HIPing times to achieve theoretical (100%) densities than low-Al_2O_3 compositions.

7. Discussion

Microstructural development and sintering mechanisms of mullite sample specimens are dependent on three variables:

(i) Al_2O_3/SiO_2 ratios of starting powders;
(ii) calcination temperatures of starting powders;
(iii) sintering temperatures and HIP conditions.

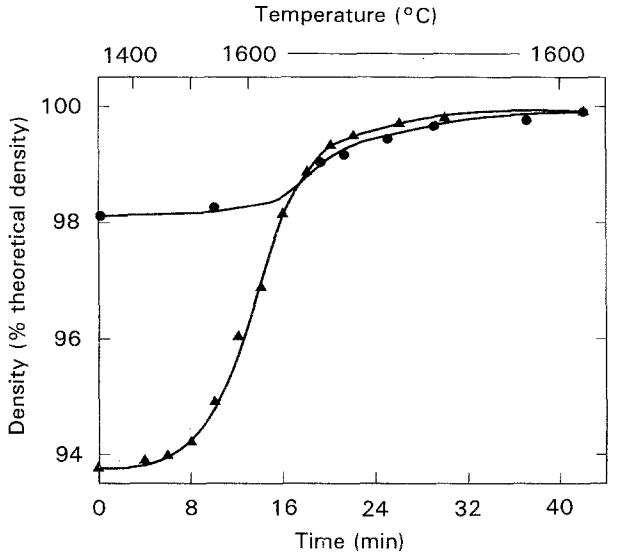

Figure 7 HIP-densification curves of (●) high-Al_2O_3 (78 wt % Al_2O_3) and (▲) low-Al_2O_3 (72 wt % Al_2O_3) materials dependent on temperature and time. Specimens are prepared from precursor powders calcined at 1100 ° C, and are sintered at 1700 ° C in air.

While Al_2O_3/SiO_2 ratios and calcination temperatures were varied systematically, sintering temperatures and HIP conditions were held constant.

Knowledge of the mullite formation mechanisms may contribute to the understanding of microstructural development and sintering mechanisms of sample specimens. Recent X-ray diffractometric and nuclear magnetic resonance (NMR) studies of Schneider *et al.* ([9,10], and unpublished results) on as-received and on heat-treated mullite precursor powders of low- and high-Al_2O_3 compositions have shown that above ≈ 900 °C, Al_2O_3-rich mullite with a composition close to that of 2/1-mullite (78 wt % Al_2O_3) is formed in both cases. This means that above ≈ 900 °C, high-Al_2O_3 materials are monophase Al_2O_3-rich mullite, whereas low-Al_2O_3 compositions consist of Al_2O_3-rich mullite plus SiO_2-rich melt. With increasing temperature, the Al_2O_3 content of mullite decreases to reach stoichiometry above ≈ 1250 °C. This causes the amount of glass phase to gradually become lower and finally it should disappear completely above ≈ 1250 °C in low-Al_2O_3 compositions. In high-Al_2O_3 compositions, the temperature-dependent decrease of the mullites' Al_2O_3 contents produces gradually increasing amounts of α-Al_2O_3 coexisting with mullite. Because there is no change in the mullites' chemical compositions between ⩾ 1250 and ⩽ 1600 °C, phase assemblages probably are stable in this temperature range. Phase diagrams may be used to understand processes at the sintering temperature (1700 °C). According to the phase diagrams published by Klug *et al.* [11,12], the stable phase assemblage of low-Al_2O_3 compositions (72 wt % Al_2O_3) at sintering temperature is mullite plus a coexisting liquid phase. High-Al_2O_3 compositions form mullite plus α-Al_2O_3.

We believe that the presence of a liquid phase in low-Al_2O_3 compositions and its absence in high-Al_2O_3 compositions, especially in the early stages of reaction sintering (between ≈ 900 and ≈ 1100 °C) has a decisive influence on sintering and on the mode and degree of mullite crystal growth and associated microstructural developments of sample specimens.

7.1. Microstructural development

Liquid-phase sintering of low-Al_2O_3 compositions produces large tabular mullite crystals embedded in a fine-grained matrix, while the equiaxed mullite microstructure with some additionally occurring α-Al_2O_3 grains of high-Al_2O_3 compositions is a result of a solid-state sintering process. The different mullite grain growth modes in high- and low-Al_2O_3 mullite compositions in turn directly influence the densification process at longer lasting heat treatments: liquid-phase reaction sintering of low-Al_2O_3 compositions does produce a stiff skeleton of interlinked elongated mullite crystals (Fig. 8). By increasing the sintering temperatures, or after longer hold times, the fine-grained matrix in between the tabular mullite network may further sinter, producing dense areas with a small number of relatively large pores. However, the stiff mullite skeleton does not allow any

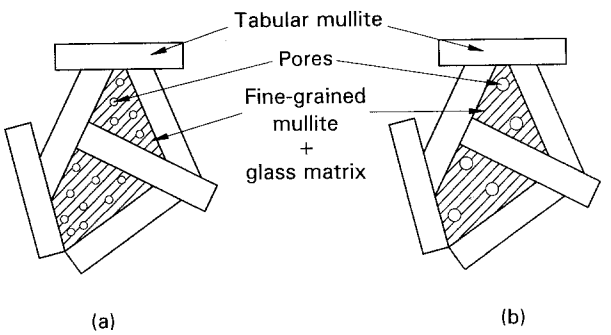

Figure 8 Stiff skeleton of tabular mullite crystals embedded in a fine-grained mullite plus glass matrix. The microstructure is typical for liquid-phase sintered low-Al_2O_3 materials (72 wt % Al_2O_3) calcined between 600 and 1100 °C. From (a) to (b) the sintering temperature increases, simultaneously the porosity decreases, though individual pores become larger.

further bulk volume shrinkage of sample specimens, thus limiting the overall densification. Solid-state sintering of high-Al_2O_3 compositions produces microstructures consisting of fine-grained equiaxed mullite plus α-Al_2O_3. Because solid-state diffusion is a temperature-dependent process, high sintering temperatures lead to higher final densities. The critical point of the procedure was to find the best sintering temperature, which in the present case lies near 1700 °C: lower temperatures do not effect sufficiently high sintering densities, and higher temperatures give rise to secondary grain growth which has an unfavourable influence on the materials' properties.

The microstructural development directly controls the mechanical properties of the materials. The interlinked network of tabular mullite crystals occurring in low-Al_2O_3 compositions produces favourable mechanical strength values by mullite–mullite (self-) reinforcement. At high temperature ($\geqslant$ 1000 °C), however, the mechanical strength falls, owing to viscous flow caused by the presence of glass phase. The equiaxed microstructure of high-Al_2O_3 compositions, on the other hand, may explain why these materials have slightly lower mechanical strengths at room temperature than low-Al_2O_3 materials. At high temperature (up to $\approx$ 1300 °C), however, the virtual absence of glass in high-Al_2O_3 compositions is favourable, because it causes preservation of the mechanical strength [13].

7.2. Sintering mechanisms

Sacks and Pask [14,15] suggested that the primary mechanism of mullite sintering is grain-boundary mass transport or diffusion, and that the sintering rates are essentially controlled by the presence or absence of liquid films around individual mullite grains. Kanzaki *et al.* [16] investigated the sintering of spray-pyrolysis produced mullite (bulk compositions 60–78 wt % Al_2O_3) and found that densification of compacts with low-Al_2O_3 contents was enhanced, which was explained by the presence of a liquid phase at sintering temperature. Ismail *et al.* [17] published data on sintering of sol–gel materials (bulk compositions 70–75 wt % Al_2O_3, calcination temperature 1400 °C) between 1600 and 1700 °C. Above $\approx$ 1650 °C, the density of all powder compacts became high, and there exists a reciprocal dependence of the sintering density on the Al_2O_3 content. Ismail *et al.* [17] explained this in a similar manner to Kanzaki *et al.* [16] by liquid-phase sintering.

The present study supports the reciprocal relationship between sintering densification and Al_2O_3 content discussed by Kanzaki *et al.* [16], Ismail *et al.* [17], and Sacks *et al.* [18] for high powder-calcination temperatures (1650 °C): in spite of similarly low surface areas (3 and 5 g cm^{-2}, Table I) of both calcined powders, the densification after sintering is much higher for low-Al_2O_3 (95.3%) than for high-Al_2O_3 compositions (85%, Table I). The former is ascribed to viscous flow densification due to the presence of glass phase. However, at lower calcination temperature ($\leqslant$ 1250 °C) relationships are just the opposite, with high-Al_2O_3 materials producing higher sintering densification than low Al_2O_3 compositions. The discrepancy of the sintering behaviour of powders calcined at relatively low temperatures is explained by the prefixing of the microstructural development during calcination. Low-Al_2O_3 compositions calcined at relatively low temperatures ($\leqslant$ 1250 °C) produce elongated mullite crystals with high aspect ratios, while high-Al_2O_3 materials form equiaxed crystals. During sintering the mullite crystals grow further but certainly without changing their contours. The densification of low-Al_2O_3 compositions thus is limited by the formation of stiff mullite skeletons, whereas high-Al_2O_3 materials show the unlimited sintering densification, as described in Section 4.2.

Sintering activity values, given as the difference between sintering and green densities, are plotted versus calcination temperatures of powders in Fig. 9.

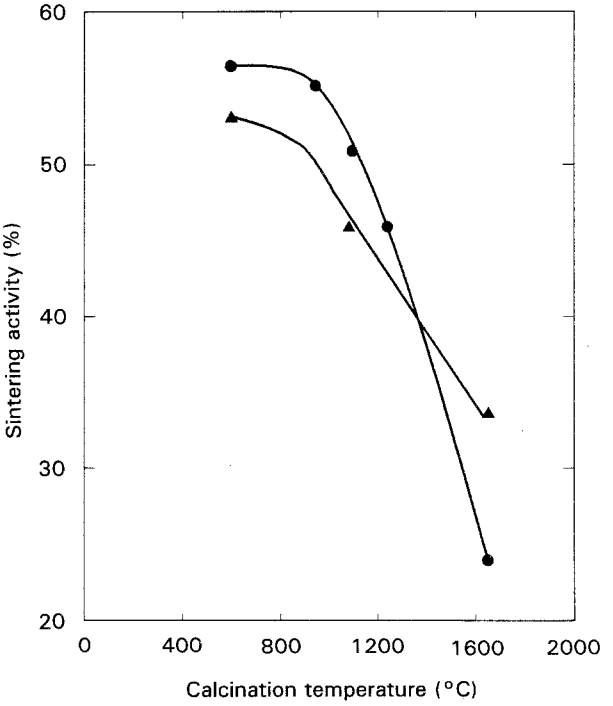

Figure 9 Sintering activity plotted as function of calcination temperatures for (●) high-Al_2O_3 (78 wt % Al_2O_3) and (▲) low-Al_2O_3 (72 wt % Al_2O_3) compositions. Sintering activities are given as the difference between sintering density and green density (Table I).

Sintering activities are highest for precursors calcined between 600 and 950 °C, but rapidly fall at higher calcination temperatures. This can be understood, taking into account that surface area values of starting powders are very high for calcination temperatures below 1100 °C. At higher calcination temperatures, they rapidly decrease to achieve very low values for samples calcined at 1650 °C (Table I). The sharp decrease of the sintering density of powders calcined above $\approx$ 1250 °C probably reflects the negative effect of particle growth, agglomerate formation, and of mullitization on sintering densification (see also [18,19]). Again there is a correlation between sintering activity and chemical composition of the materials: low-Al_2O_3 compositions exhibit a flatter calcination temperature-dependent decrease of the sintering activities than high-Al_2O_3 compositions. This is explained by the virtual absence of a liquid phase in the high-Al_2O_3 compositions, but with the presence of such a phase in the former case. Coexisting liquid phases enhance diffusion-controlled sintering, and in that way work against the reduction of the sintering activity.

Differentiated dilatometer curves were used to obtain further information on the sintering process. The curves for high- and low-Al_2O_3 compositions measured under an oxidizing (air) atmosphere yield a minimum of the shrinkage rates near 1320 °C (Fig. 10). Under the reducing atmosphere of the HIP furnace, a second, quite strong, minimum of the densification rate near 1550 °C does occur. Under oxidizing conditions this effect is very weak for low-Al_2O_3 compositions, while it is not observed at all in high-Al_2O_3 materials. Rodrigo and Boch [20,21] observed intense cristobalite formation in the former temperature range, and attributed the sharp decrease of corresponding shrinkage rates to the crystallization of amorphous SiO_2 coexisting with mullite to cristobalite. Our own X-ray diffraction patterns collected from powders heat-treated in a similar way as during corresponding dilatometer runs, and which were quenched to room temperature, yield no evidence for cristobalite but a discontinuous increase of the mullite content between 1250 and 1350 °C. Therefore, the lowering of the sintering rate near 1320 °C is correlated to volume increase induced by mullitization, which works against the sintering-induced shrinkage. At present we have no clear idea for the explanation of the sintering minimum at about 1550 °C. However, it can be stated that the effect is intensive for low Al_2O_3 compositions, especially under reducing sintering atmospheres. It may, therefore, be associated in some way with the glass phase occurring in that composition. Perhaps solution of the smaller sized mullite grains in the coexisting melt and subsequent nucleation and growth of larger tabular crystals is one reason for it.

Relative HIP-induced densification curves of high- and low-Al_2O_3 mullite compositions are plotted in Fig. 11. The low-Al_2O_3 materials' curve is steeper, and approaches theoretical density (100%) more rapidly

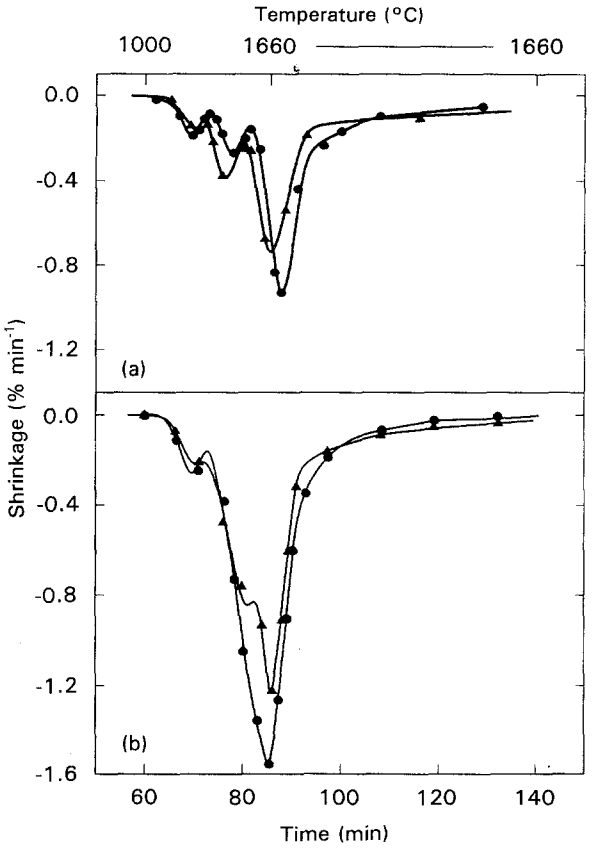

Figure 10 Derived shrinkage values of (●) high-Al_2O_3 (78 wt % Al_2O_3) and (▲) low-Al_2O_3 (72 wt % Al_2O_3) materials dependent on temperature and time. Specimens are prepared from precursor powders calcined at 1100 ° C. The curves were recorded in (a) nitrogen and (b) air atmospheres.

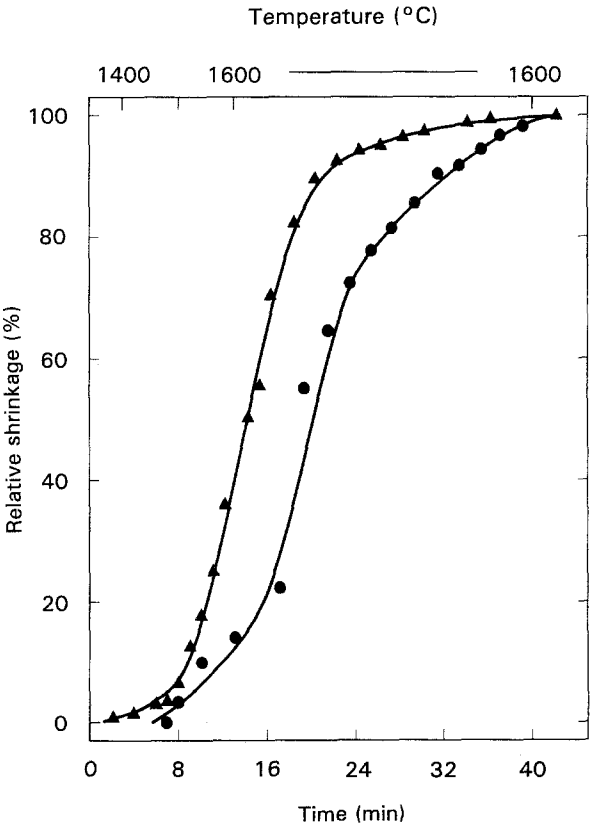

Figure 11 Relative HIP-shrinkages of (●) high-Al_2O_3 (78 wt % Al_2O_3) and (▲) low-Al_2O_3 (72 wt % Al_2O_3) materials dependent on temperature and time. Specimens are prepared from precursor powders calcined at 1100 ° C and are sintered at 1700 ° C in air.

than high-Al_2O_3 compositions. Furthermore, the shrinkage curve is shifted towards lower temperature with respect to the high-Al_2O_3 curve. Two main reasons may be responsible for the different HIP-densification curves of high- and low-Al_2O_3 materials: low-Al_2O_3 materials have lower pre-HIP densities (93.8%) than high-Al_2O_3 materials (98.2%). Consequently, low-Al_2O_3 sample specimens can be HIP-densified more easily than high-Al_2O_3 compositions. Furthermore, low Al_2O_3 mullite materials contain significantly larger amounts of glass phase than high Al_2O_3 compositions. Therefore, pressure-aided viscous flow is a main driving force for rapid HIP-densification in the case of low-Al_2O_3 compositions, whereas slower solid-state diffusion-controlled HIP-sintering is a main factor of the latter.

8. Conclusions

An important conclusion of our recent investigations was that sintering mechanisms and associated development of microstructures of mullite ceramics produced from coprecipitated precursor powders is controlled by varying the Al_2O_3/SiO_2 ratio, and by using different calcination procedures of the starting mullite precursor powders: completely dense, homogeneous and fine-grained mullite microstructures necessary for mullite substrates and for optical windows can be processed using suitable calcination, sintering and HIPing conditions from high-Al_2O_3 starting materials. Completely dense and homogeneous, self-reinforced microstructures, consisting of a skeleton of tabular mullite crystals, and a fine-grained mullite matrix, required for structural application can be processed using suitable calcination, sintering and HIPing conditions from low-Al_2O_3 compositions. The latter have good mechanical properties at room temperature [13]. The materials should also be suitable for applications at high temperature, if the glass phase occurring at the interface of tabular mullite crystals is eliminated by recrystallization, e.g. by addition of Y_2O_3 or MgO. Further experimental work will be concerned with this aim.

Acknowledgements

Sample materials were provided by Dr. Maschmeyer, Huls Company (Marl, Germany) with grateful acknowledgement. We thank Mr H. Hermanns (DLR, Köln) for technical assistance.

References

1. T. AKSAY, D. M. DABBS and M. SARIKAYA, *J. Am. Ceram. Soc.* **74** (1991) 2343.
2. J. D. HEAPS, S. B. SCHULDT, B. L. GRUNG, J. D. ZOOK and C. D. BUTTER, in "IEEE Proceedings of the 30th Electronic Components Conference" (1980) pp. 39–48.
3. G. CELOTTI, L. MORETTINI and G. ORTELLI, *J. Mater. Sci.* **18** (1983) 1005.
4. S. PROCHAZKA and F. J. KLUG, *J. Am. Ceram. Soc.* **66** (1983) 874.
5. R. F. DAVIS and J. A. PASK, in "Refractory Materials. High Temperature Oxides", Part IV, Refractory Glasses, Glass-Ceramics, and Ceramics, edited by A. M. Alper (Academic Press, New York, London, 1971) pp. 37–76.
6. J. A. PASK and A. P. TOMSIA, *J. Am. Ceram. Soc.* **74** (1991) 2367.
7. S. SOMIYA and Y. HIRATA, *Ceram. Bull.* **70** (1991) 1624.
8. H. SCHNEIDER, Habilitationsschrift, Faculty of Chemistry, University of Münster, Germany (1986).
9. H. SCHNEIDER, L. MERWIN and A. SEBALD, *J. Mater. Sci.* **27** (1992) 805.
10. H. SCHNEIDER, B. SARUHAN, D. VOLL, L. MERWIN and A. SEBALD, *J. Eur. Ceram. Soc.*, **11** (1993) 87.
11. F. J. KLUG, S. PROCHAZKA and R. H. DOREMUS, *J. Am. Ceram. Soc.* **70** (1987) 750.
12. F. J. KLUG, S. PROCHAZKA and R. H. DOREMUS, *Ceram. Trans.* **6** (1990) 15.
13. B. KANKA and H. SCHNEIDER, unpublished results.
14. M. D. SACKS and J. A. PASK, *J. Am. Ceram. Soc.* **65** (1982) 65.
15. *Idem, ibid.* **65** (1982) 70.
16. S. KANZAKI, H. TABATA, and T. KUMAZAWA, *Ceram. Trans.* **6** (1990) 339.
17. M. G. M. U. ISMAIL, Z. NAKAI and S. SOMIYA, *ibid.* **6** (1990) 231.
18. M. D. SACKS, H. LEE and J. A. PASK, *ibid.* **6** (1990) 167.
19. Y. HIRATA and K. SHIMADA, in "Mullite", edited by S. Somiya (Uchida Rokakuho, Tokyo, Japan, 1985) pp. 89–122.
20. P. D. D. RODRIGO and P. BOCH, *Int. J. High Technol. Ceram.* **1** (1985) 3.
21. *Idem, J. Phys.* **47** (1986) C1-411, C1-416.

Received 24 August 1992
and accepted 20 August 1993